

Reaction of a polar gravel-spit system to atmospheric warming and glacier retreat as reflected by morphology and internal sediment geometries (South Shetland Islands, Antarctica)

Pablo Heredia Barión,^{1,2*}  Sebastian Lindhorst,³ Ilona Schutter,³ Ulrike Falk¹ and Gerhard Kuhn¹

¹ Helmholtz Center for Polar and Marine Research, Geosciences Division, Alfred Wegener Institute, Am Alten Hafen 26, 27568 Bremerhaven, Germany

² Department of Geosciences, University of Bremen, Klagenfurterstr, 2-4, 28359 Bremen, Germany

³ University of Hamburg, Institute for Geology, Bundesstr, 55, 20146 Hamburg, Germany

Received 16 February 2018; Revised 7 November 2018; Accepted 22 November 2018

*Correspondence to: Pablo Heredia Barión, Alfred Wegener Institute, Helmholtz Center for Polar and Marine Research, Geosciences Division, Am Alten Hafen 26, 27568 Bremerhaven, Germany. E-mail: pablo.heredia@awi.de

This is an open access article under the terms of the Creative Commons Attribution License, which permits use, distribution and reproduction in any medium, provided the original work is properly cited.

ESPL

Earth Surface Processes and Landforms

ABSTRACT: Sedimentary architecture and morphogenetic evolution of a polar bay-mouth gravel-spit system are revealed based on topographic mapping, sedimentological data, radiocarbon dating and ground-penetrating radar investigations. Data document variable rates of spit progradation in reaction to atmospheric warming synchronous to the termination of the last glacial re-advance (LGR, 0.45–0.25 ka BP), the southern hemisphere equivalent of the Little Ice Age cooling period. Results show an interruption of spit progradation that coincides with the proposed onset of accelerated isostatic rebound in reaction to glacier retreat. Spit growth resumed in the late 19th century after the rate of isostatic rebound decreased, and continues until today. The direction of modern spit progradation, however, is rotated northwards compared with the growth axis of the early post-LGR spit. This is interpreted to reflect the shift and strengthening in the regional wind field during the last century. A new concept for the interplay of polar gravel-spit progradation and glacio-isostatic adjustment is presented, allowing for the prediction of future coastal evolution in comparable polar settings. © 2018 The Authors. Earth Surface Processes and Landforms published by John Wiley & Sons Ltd.

KEYWORDS: ground-penetrating radar; polar gravel beaches; glacio-isostatic adjustment; deglaciation; Antarctic Peninsula

Introduction

A spit is a wave-built sediment body attached to a headland on one end and terminating in open waters on the other (Evans, 1942). Gravel spits prograde by arcuate-shaped accretion of gravel ridges (Bluck *et al.*, 2001). Among other morphologies of barrier coasts, they are typical for comparable sheltered coastal environments and tend to be best developed in areas where short-period waves approach the coast at a high angle (Otvos, 2012; Cooper *et al.*, 2015). In high latitudes, spits often consist of cobbles and boulders derived from moraines in upstream direction. Periglacial and polar beach systems are subjected to glacio-isostatic movements and consequently varying relative sea level. This results in a complex sedimentary architecture due to shifts in sediment supply and depocenters (Orford *et al.*, 2002), as well as, the accommodation space, i.e. the space which is available for sedimentation. Polar beach systems are valuable archives of sea level, past sea-ice conditions as well as the wave- and storm climate (Baroni and Orombelli, 1991; Møller *et al.*, 2002; Hall and Perry, 2004;

Santana and Dumont, 2007; Mason, 2010; St-Hilaire-Gravel *et al.*, 2010, 2015; Lindhorst and Schutter, 2014; Simkins *et al.*, 2015; Nielsen *et al.*, 2017).

Morphodynamics of gravel-spit formation in mid-latitude settings is well understood (Forbes and Taylor, 1987; Forbes *et al.*, 1995; Tamura, 2012; Bujalesky and Gonzalez Bonorino, 2015; Burningham, 2015). The same is valid for the involved main controlling factors: coast-oblique incident waves that cause a significant longshore drift, the availability of a sediment source in the up-drift direction, and wave refraction around the growing tip of the spit leading to a reduction in alongshore-transport capacity and, as such, triggering sedimentation (Bluck *et al.*, 2001; Nielsen and Johannessen, 2009). However, only few studies have focused on the dynamics of gravel beaches in polar regions (St-Hilaire-Gravel *et al.*, 2012, 2015; Lindhorst and Schutter, 2014; Strzelecki *et al.*, 2015, 2018) and there still is a gap in knowledge on the evolution, the sedimentary dynamics and the resulting internal architecture of gravel-spit systems developed under the circumstances of rapid atmospheric warming and associated changes of wind climate and relative

sea level. This study aims at filling this gap by revealing the genesis of, and by providing a concept for, the evolution of polar gravel-spit systems that developed during a phase of accelerated deglaciation and subsequent crustal isostatic adjustment.

Regional setting

Study site

The studied spit is about 350 m wide and 280 m long, and located at the mouth of Potter Cove, a tributary fjord of Maxwell Bay situated in the SW of King George Island (Figures 1–3). King George Island (KGI, 62° 23' S, 58° 27' W) is the largest of the South Shetland Islands (SSI), located 120 km NW of the Antarctic Peninsula (AP). The Drake Passage towards the NW and the Bransfield Strait towards the SE frame the island group. About 90% of the island is covered by the Collins Ice Cap, which elevates to 700 m above present mean sea level (amsl)

(Rückamp *et al.*, 2011; Osmanoglu *et al.*, 2013). Outcropping bedrock and moraines, and active and raised beaches characterize the ice-free areas on KGI. The Potter Cove spit system stands exemplarily for similar systems along the coasts of the SSI and elsewhere (Figure 4).

Potter Cove is about 4 km long and 2.5 km wide with a recently stranded tide-water glacier located at the head of the cove. Water depths in the inner cove are up to 50 m and exceed 100 m in the outer cove (Schloss *et al.*, 2012). In the surroundings of the spit, water depths reach 20 m (Deregibus *et al.*, 2015; Figure 1(C)). The tidal range is about 1.2 m during neap and 1.5 m during spring tide (Schoene *et al.*, 1998).

Atmospheric and marine climate

Average sea-surface temperature in Potter Cove reaches 1°C during the summer months, and has increased by 0.36°C per decade during the past two decades (Schloss *et al.*, 2012). Maxwell Bay and Potter Cove are generally free of sea ice from

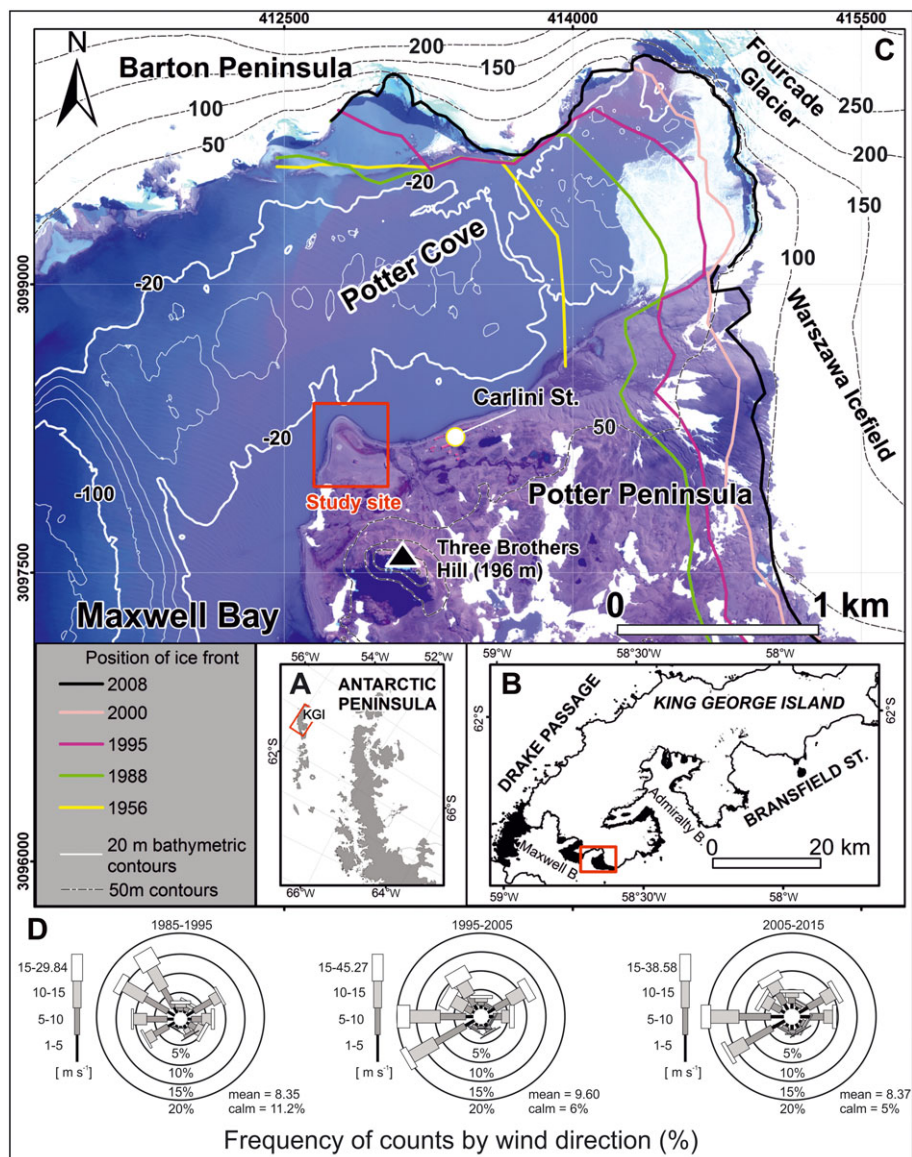


Figure 1. Location of studied spit system. (A) King George Island (KGI) belongs to the South Shetland Islands, west of the Antarctic Peninsula. (B) KGI is framed by the Drake Passage and the Bransfield Strait. Ice-free areas (black) are limited to the coastal zone, whereas the inland is glaciated (white); box marks the position of Potter Peninsula. (C) Satellite image of Potter Peninsula with location of the Potter Cove spit system (box). Past ice front positions are from Rückamp *et al.* (2011); bathymetric data from Deregibus *et al.* (2015). (D) Wind data for the 1985–2015 CE observational period. [Colour figure can be viewed at wileyonlinelibrary.com]

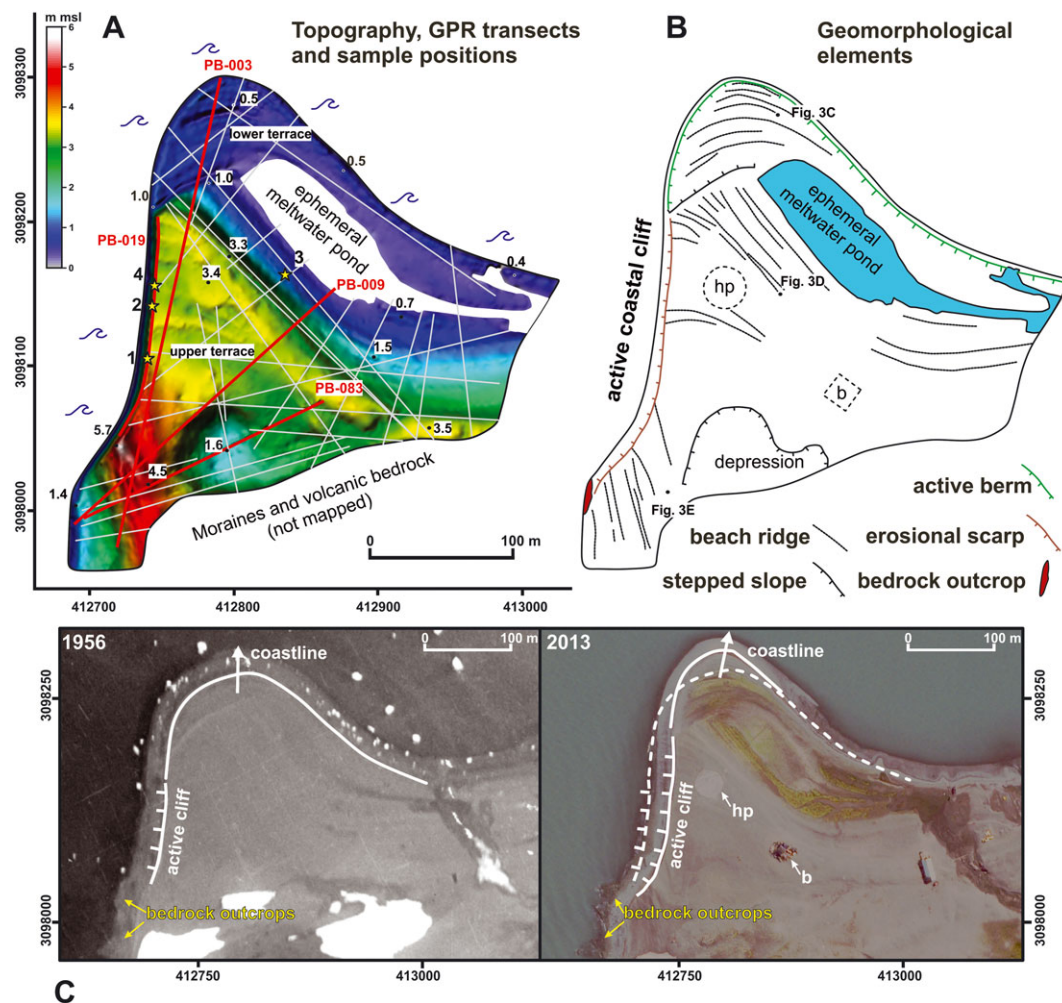


Figure 2. Topography and geomorphology of Potter Cove spit system. (A) Digital terrain model based on dGPS measurements (numbers refer to elevation in meters above mean sea level). Note upper and the lower terrace, and the position of GPR transects (lines presented in the text are marked in red); yellow stars mark sample positions for radiocarbon dating. (B) Geomorphological elements of the spit system. Figure numbers refer to surface photographs; hp: heliport; b: building. (C) Aerial and satellite imagery of the spit system, taken in 1956 and 2013 respectively. White arrows indicate the direction of spit progradation. [Colour figure can be viewed at wileyonlinelibrary.com]

November/December to April/May; open waters in the Bransfield Strait last from December to April (Griffith and Anderson, 1989; Yoon *et al.*, 1997; Schloss *et al.*, 2012). The wind field in the study area is W–E bi-directional, with predominant winds from SW to NW and from NE to SE; average wind speed is about 15 m s^{-1} (Braun *et al.*, 2001; Bañón *et al.*, 2013; Schloss *et al.*, 2014; Falk and Sala, 2015; SMN, 2016; Figure 1D). SW to NW winds are more common during the austral summer, whereas NE to E winds are weaker and less common. However, local scale wind patterns, especially in fjords and coves, are strongly influenced by the surrounding topography (Braun *et al.*, 2004; Navarro *et al.*, 2013; Falk and Sala, 2015).

The southern and western coasts of Potter Peninsula including the western coast of the spit are exposed to oceanic waves coming from the Bransfield Strait (Figures 1 and 3(A)). During open-water seasons, the predominant direction of incident waves is oblique to the coast from S to SW creating a northward-flowing longshore current (Lim *et al.*, 2013). Waves are refracted at the entrance of Potter Cove and bend around the spit into the cove, where wave energy decreases. During westerly storms, waves at the entrance of the cove reach a height of up to 1.7 m, whereas waves in the inner cove are 50–40% lower (Lim *et al.*, 2013). The wave climate of Potter Cove is strongly influenced by local wind conditions and only subjected to minimal swell energy (Lim *et al.*, 2013). Fetch

inside Potter Cove is very limited and, as a result, even strong easterly winds cannot create significant wave heights.

KGI is subjected to a maritime climate and regularly hit by cyclonic weather systems moving eastward along the Drake Passage (Kejna *et al.*, 2013). The strength of circumpolar westerly winds has increased since the 1970s, especially during the austral summer, accompanied by higher cloudiness and precipitation (van den Broeke, 2000; Turner *et al.*, 2005; Stammerjohn *et al.*, 2008; Montes-Hugo *et al.*, 2009). The annual mean air temperature on KGI during the time period 1948 to 2011 CE was -2.5°C (Kejna *et al.*, 2013), but temperatures are often above zero during summer. Average annual air temperatures above the AP have increased rapidly by up to 3°C in the second half of the last century, causing an accelerated glacier retreat (Cook *et al.*, 2005; Meredith and King, 2005; Vaughan, 2006).

Holocene deglaciation and sea-level history

The deglaciation of Potter Cove initiated somewhat after 1.6 ka cal BP (Wöfl *et al.*, 2016). Along the coasts of the SSI, Holocene raised beaches occur up to elevations of 18 m amsl (John and Sugden, 1971; Fretwell *et al.*, 2010; Hall, 2010; Simms *et al.*, 2012). Beach uplift on the SSI results from crustal

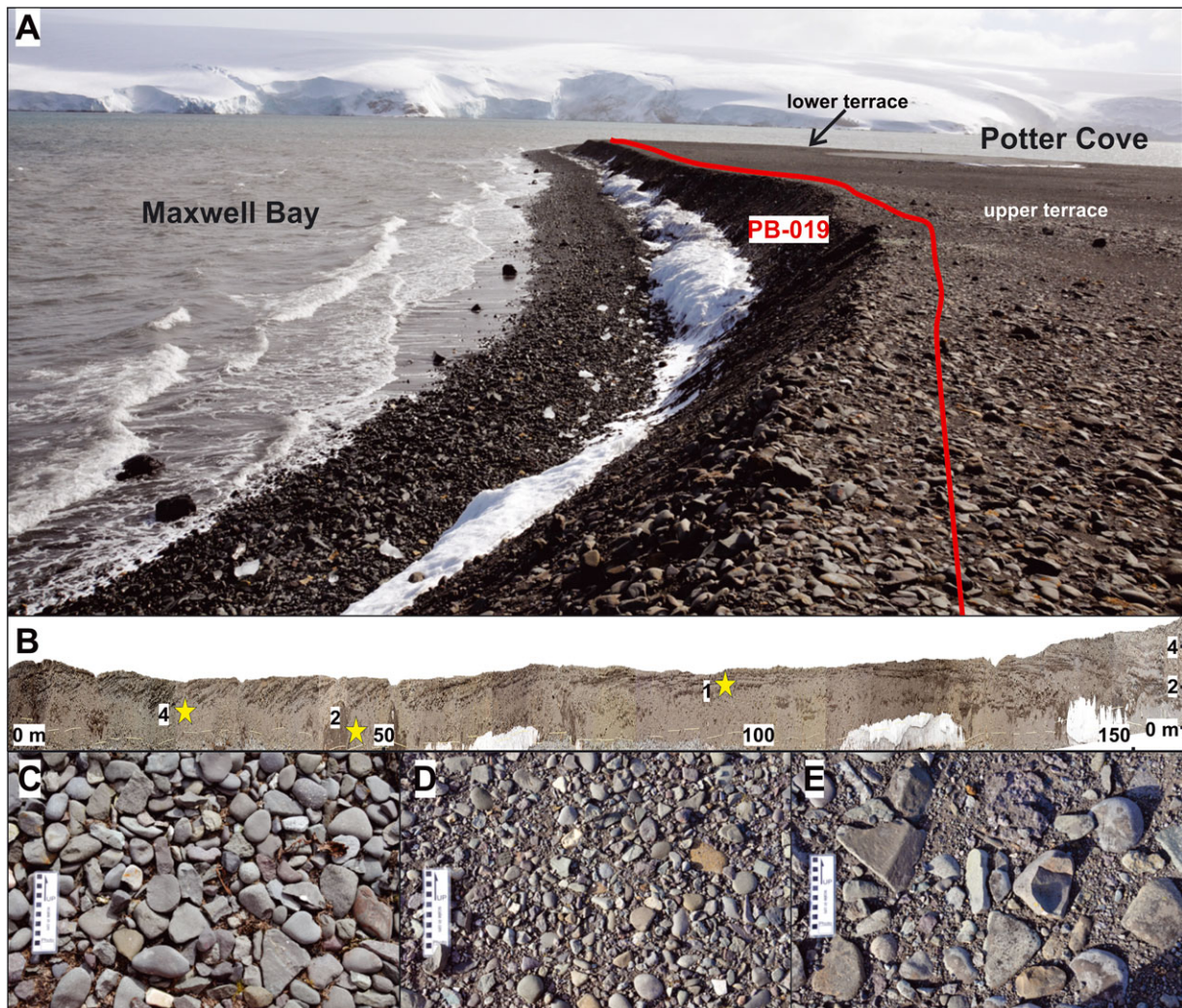


Figure 3. (A) View along the west coast of the spit looking north. Height of cliff is up to 5 m. Positions of GPR transect PB-019 and the lower and upper terrace are shown. (B) Panorama of cliff section showing internal sedimentary bedding and position of dated samples. Elevations are in m amsl. (C, D, E) Images of surface sediment texture; see Figure 2 for locations. [Colour figure can be viewed at wileyonlinelibrary.com]

relaxation in reaction to decreasing ice load following the Last Glacial Maximum (John and Sugden, 1971; Bentley *et al.*, 2005; Fretwell *et al.*, 2010; Watcham *et al.*, 2011; Ó Cofaigh *et al.*, 2014). Raised beaches along the coasts of Maxwell Bay, located at 7.5 to 4 m amsl (locally termed '6-m-beaches'), interfinger with terminal moraines of the last glacial-readvance (LGR), which occurred between 0.45 and 0.25 ka cal BP (John and Sugden, 1971; Sugden and John, 1973; Clapperton and Sugden, 1988; Yoo *et al.*, 2004; Yoo *et al.*, 2009; Simms *et al.*, 2012). It is therefore likely that these beaches developed during the LGR (John and Sugden, 1971; Sugden and John, 1973; Hall, 2010).

Recent uplift of KGI was 0.4 mm a^{-1} during the last decade (Rülke *et al.*, 2015). Average uplift during the entire Holocene, however, is 2.8 to 3 mm a^{-1} (Bentley *et al.*, 2005; Fretwell *et al.*, 2010). Fall of relative sea level on KGI accelerated during the last 500 years (Bentley *et al.*, 2005; Hall, 2010; Watcham *et al.*, 2011). This was most likely the result of a short-term acceleration in glacio-isostatic rebound after the LGR, with a modeled peak uplift rate of 12.5 mm a^{-1} between 1700 and 1840 CE (Simms *et al.*, 2012).

There are numerous sea-level curves for the SSI, derived from dating of raised beaches, marine abrasion terraces, and isolation basins (Pallàs *et al.*, 1997; Bentley *et al.*, 2005; Hall, 2010; Watcham *et al.*, 2011). However, Holocene ice retreat and resulting fall of relative sea level was not a continuous

process (Simms *et al.*, 2011). Bentley *et al.* (2005) show that an initial post-glacial sea-level fall was interrupted by a mid-Holocene highstand at about 14.5 to 16 m amsl from 5.8 to 3.0 ka cal BP. In contrast, data presented by Hall (2010) show a continuous sea-level fall, which becomes accelerated between 1.5 and 0.5 ka cal BP. Watcham *et al.* (2011) presented a sea-level curve based on data from isolation basins and raised beaches. This curve shows two mid-Holocene sea-level highstands for KGI at about 8.0 and 7.0 ka cal BP, and a subsequent sea-level fall due to long-term glacio-isostatic rebound. Simms *et al.* (2012) mentioned that most sea-level curves for the SSI indicate an accelerated fall over the past 2.0 ka cal BP, whereas sea-level records from regions along the western AP reflect a decrease in uplift rate over time.

Methods

Topographic mapping

Data on ridge and terrace elevations, required for spit-system mapping and for the topographic correction of ground-penetrating radar data, were collected using a Leica GS09 differential GPS (dGPS) in either RTK rapid static or RTK kinematic mode (3D-accuracy of better 2 cm). As geodetic reference, the point DALL 66019 M002 ($S62^{\circ}14'16.335''/W58^{\circ}39'52.364''$)

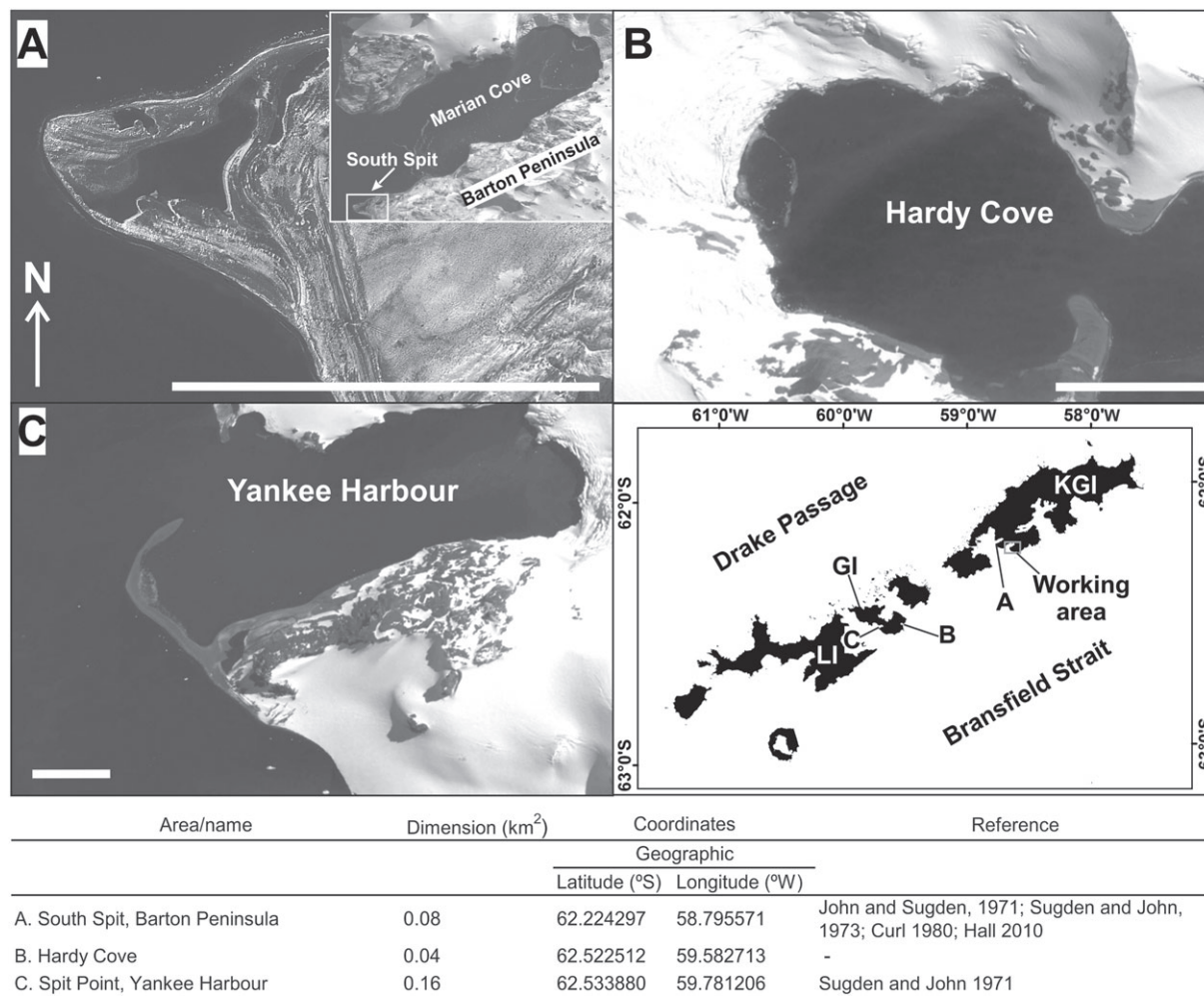


Figure 4. Selection of other gravel spits of the South Shetland Islands, comparable with the Potter Cove System. GI: Greenwich Island; LI: Livingston Island. Scale bars represent 500 m in each picture. Satellite images (Google Earth) are from 2011 (A, B), and from 2010 (C).

ellipsoidal height 39.376 m) located on Carlini (formerly Jubany) Station was used. All UTM coordinates refer to zone 21E and are based on the WGS84 ellipsoid. No fixed tidal datum exists for the working area due to the lack of long-term water-level observations. Measured WGS84 ellipsoid heights were therefore corrected for the geoid undulation of $-22.00 \text{ m} \pm 0.10 \text{ m}$ using the data of the EGM96 (Lemoine *et al.*, 1998). A geoid height of zero is taken as local vertical datum and referred to as present mean sea level (msl).

Ground-penetrating radar

Ground-penetrating radar (GPR) is based on the transmission of high-frequency electromagnetic pulses that are partly reflected at electromagnetic discontinuities in the subsurface. The amplitude of the reflected signal is recorded as a function of the two-way-travel time (TWT). GPR always images an interference pattern caused by the thickness of individual electromagnetically uniform sediment packages and the wavelengths present in the GPR signal (Lindhorst and Schutter, 2014). GPR data for this study were acquired by means of a GSSI (Geophysical Survey Systems Inc.) SIR-3000 GPR with a 200 MHz antenna; operated in discrete mode (trace increment 0.05 m). Post-processing of GPR data using the software ReflexW (Sandmeier Geo) comprises data editing, subtraction of low-frequency signal components (dewow), frequency filtering, gain adjustment, topographic migration and correction for along-profile topography. A mean subsurface radar-wave velocity of 0.08 m ns^{-1} was

determined based on the analysis of diffraction hyperbolae. Interpretation of GPR data is based on migrated as well as non-migrated data, the latter being essential for a correct tracing of ringing multiples and diffraction hyperbolae. Only non-migrated data are shown in this work. Data interpretation follows the approach of radar-facies interpretation (Gawthorpe *et al.*, 1993; Bristow, 1995) as applied by Lindhorst *et al.* (2008) to spit sediments of lower latitudes. Analogous to the concepts of seismic interpretation introduced by Mitchum *et al.* (1977), the term 'radar facies' describes a two- or three-dimensional set of reflections with similar characteristics, bordered by 'radar surfaces' (Bristow, 1995). Consequently, the interpretation of unconformities is based on the tracing of reflection terminations and abrupt changes of the radar facies.

Absolute age determination

Absolute age data were obtained by AMS radiocarbon dating of seaweed and a penguin bone. To reduce the risk of contamination with modern material, all samples for dating were taken from fresh outcrops, at least 0.3 m below the surface, packed in zip-lock bags and stored at 4°C. Sample preparation and measurement as well as correction for carbon isotope fractionation and calculation of conventional radiocarbon ages (CRA) were performed by Beta Analytic Inc., USA. Local reservoir corrections (ΔR) for marine samples as reported for the SSI are in a broad range of about 700 to 1100 years (Curl, 1980; Björck *et al.*, 1991; Berkman and Forman, 1996; Milliken *et al.*,

2009; Hall *et al.*, 2010; Hass *et al.*, 2010; Watcham *et al.*, 2011). Hall *et al.* (2010), based on paired radiocarbon and uranium–thorium dates of Antarctic solitary corals, proposed a ΔR of 791 ± 121 years. This local reservoir age is further supported by results of Simms *et al.* (2012) who used optical-stimulated luminescence dating of cobble surfaces to investigate the depositional ages of beach ridges on KGI. Due to the verification with two independent dating methods, the local reservoir correction proposed by Hall *et al.* (2010) was used in this study. Calibration of conventional radiocarbon ages was done using the software Calib (v7.0.4, Stuiver and Reimer, 1993) and the calibration curve Marine13 (Reimer *et al.*, 2013). Calibrated ages are rounded to the next decade and provided as median of the probability distribution with 2σ error range (95.4% probability).

Historical aerial imagery

To reconstruct coastal evolution through time, an orthorectified panchromatic aerial image (Falkland Island Dependency Aerial Survey Expedition, FIDASE; image ID X26FID0039076; pixel resolution 0.9 m; acquired 1956/12/20) and a satellite scenery (WorldView2, DigitalWorld; scene ID: 103001001F612100; pixel resolution 0.5 m; acquired 2013/03/07) were georeferenced and compared with regard to coastline position as marked by the location of the active berm. The berm was chosen as local reference to minimize errors potentially induced by tidal water-level oscillations.

Data on wind speed and direction

Carlini Station (National Meteorological Service of Argentina) is located at 15 m amsl and 600 m away from the spit system (Figure 1). Continuous meteorological observations are available from May 1985. They encompass 3-hourly measurements of surface air temperature, wind direction and velocity, barometric sea-level pressure and cloudiness (SMN, 2016). The data are available from SCAR READER (Turner *et al.*, 2004). Data on wind direction and velocity are analyzed for sea-ice free months (November–April) with respect to decadal summaries of wind statistics (Figure 1(D)).

Results

Morphology

The Potter Cove spit is attached to a headland composed of volcanic rocks and glacial moraines (Figures 1 and 2(A)). Two terrace levels are present, here termed lower and upper terrace, connected by a slope facing north. This slope is characterized by superimposed ridges that create a stairways morphology (overall slope 5° ; Figure 2(A), (B)). Towards Maxwell Bay, there is an up to 5 m high active cliff, whereas an active gravel berm ridge frames the modern beach towards the interior of Potter Cove (Figure 2(B)). From W to E, the height of the berm ridge decreases from 1 to 0.4 m amsl.

The upper terrace (situated at 3 to 5.7 m amsl) exhibits a series of curved, NNW–SSE to NW–SE striking, morphological ridges, towards the W truncated by the cliff (Figure 3(A)). The height difference between swales and adjacent ridge crests is less than 0.6 m in the SW and less than 0.2 m on the rest of the terrace. The upper terrace slightly descends towards the NE with an overall slope of 0.6° .

The lower terrace is located at and below 0.8 m amsl. Ridge crests on this terrace are located at 0.4 to 0.8 m amsl and ridges are curved with their convex side facing N (Figure 2(B)). Ridge elevations are less than 0.2 m. The landward, S-slope of the lower terrace, measured over all the ridges is 0.2° , with a maximum of 0.6° .

Sedimentology

Grain sizes along the modern beach and on the spit range from sand to gravel. Sediments are in general poorly sorted (Figure 3(C)–(E)). However, well sorted gravel sheets occur in the modern swash zone. Ridges of the lower terrace are composed of rounded to well-rounded (according to the classification scheme by Tucker, 1996) cobbles, with a maximum grain size of 12 cm and an almost matrix-free texture (Figure 3(C)). Sediments of the upper terrace coarsen from the NE to the SW (increase in maximum grain size from 5 to 20 cm), accompanied by a trend towards better rounding and less matrix content. Most gravels at the surface and in the uppermost part of the sediment column are gelifracted with sharp angular edges (Figure 3(E)).

Spit internal sediment geometries

Out of 29 GPR lines, four were selected to document the internal architecture of the spit system (Figures 2(A) and 5–8). Seven radar facies (rf) and three radar surfaces (rs) were defined to classify the radar-reflection patterns and to deduce the sedimentary geometries (Table I). The spit system comprises two distinct units. The upper unit, Unit 1, is characterized by clear GPR reflections and unconformably overlies the lower Unit 2, which shows irregular reflections (rf IRR-B), diffraction hyperbolas, and pronounced ringing multiples. Units are seen to represent the sediments of the spit overlying the basement respectively. The contact between the two units elevates towards the SSW. In the GPR data, this contact is irregular and poorly defined with the exception of the southwestern part of the study area, where a clear contact (rs3) is imaged (Figures 5 and 6).

Sediments of the spit (Unit 1) have a thickness of 1 to 3.5 m, with lower values in the central part of the spit and higher values in the SW, where morphological ridges are superimposed on the upper terrace. Internally, tabular, continuous reflections (rf IS-A) predominate, dipping radially from the presumed spit axis towards the shores (Figures 5 and 6). These reflections are bundled into packages by erosional unconformities, characterized by the truncation of underlying reflections (rs1; Figures 5, 6 and 8). Morphological ridges of the upper terrace show convex curved reflections of low to high amplitude (rf CU), bounded by seaward-dipping unconformities (rs1) as well as tabular to slightly convex reflections of medium to high amplitude (rf IL), bounded by landward-dipping unconformities (Figures 6 and 7). The central part of the spit system is dominated by irregular, low- to high-amplitude reflections with numerous diffraction hyperbolas (rf IRR-A). Near the surface, slightly concave, low- to medium-amplitude reflections occur (rf H; Figures 5–7).

Historical coastline development and wind-field evolution

Historical aerial and satellite imagery shows that the active cliff on the W side of the spit system retreated by 20 m in the time

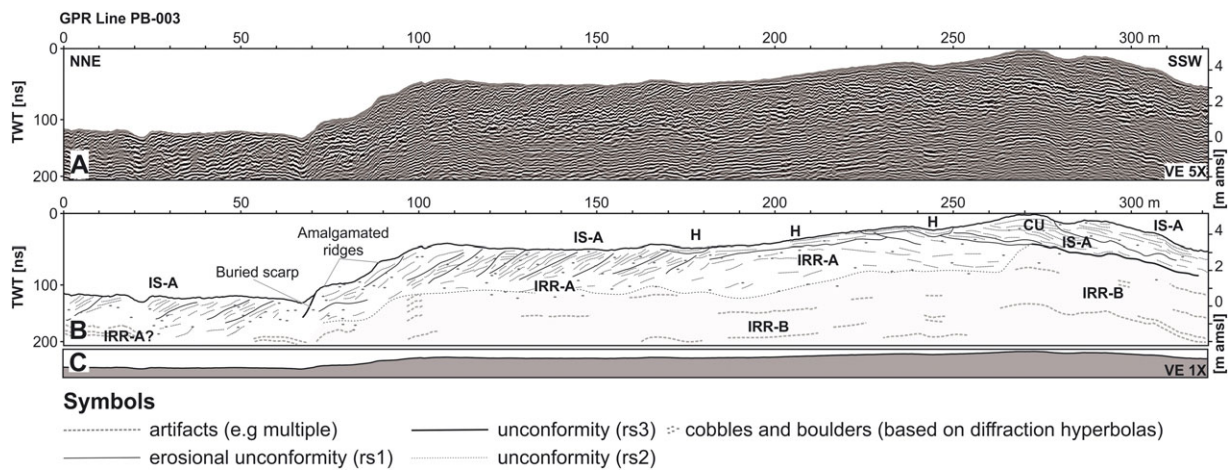


Figure 5. (A) GPR line PB-003 showing the internal architecture of the lower and upper terrace of the spit system. For location see Figure 2. (B) Interpretation of (A). For a detailed discussion of radar facies and sediment geometries see text and Table I. (C) Along-transect topography without vertical exaggeration (VE). [Colour figure can be viewed at wileyonlinelibrary.com]

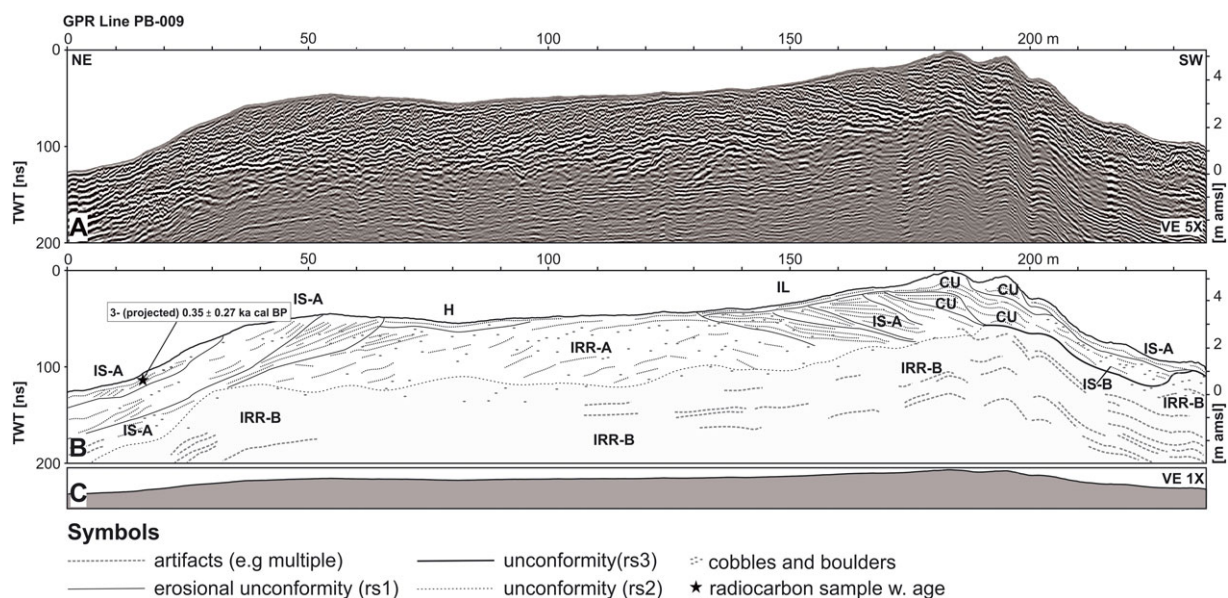


Figure 6. (A) GPR line PB-009. For location see Figure 2. (B) Interpretation of (A). For a detailed discussion of radar facies and sediment geometries see text and Table I. (C) Along-transect topography without vertical exaggeration. [Colour figure can be viewed at wileyonlinelibrary.com]

period 1956 to 2013 CE. Simultaneously, the northern coastline prograded by 25 m towards the NNE (linearly averaged rate of progradation is 0.44 m a^{-1} ; Figure 2(C)). In the year 1956 the front of the Potter Cove tide-water glacier was located 1200 m away from the gravel spit inside the cove (Figure 1(C)). Since then the glacier front has experienced a net retreat of more than 1000 m along the flow line and stepped back onto land in the year 2016 (Jerosch *et al.*, 2018).

The direction of predominant winds in the Potter Cove area changed from NW to W-SW over the last 30 years (Figure 1(D)). Moreover, the study site became stormier, with >20% of W-SW winds exceeding 15 m s^{-1} and a general increase in maximum wind speed in more recent times (c. 30 m s^{-1} in the time period 1985–1995, and 3845 m s^{-1} in the subsequent decade 1995–2015).

Discussion

Bay-mouth spit systems like the Potter Cove spit, are common morphological features along the periglacial coasts of the SSI,

where they developed at the entrances of coves and embayments (Figure 4). These entire systems exhibit superimposed beach ridges, and most comprise several terrace levels, separated by slopes or truncated by erosional scarps (John and Sugden, 1971; Sugden and John, 1973; Curl, 1980; Hall, 2010). Data on the internal architecture of these systems is missing. Similarities in overall morphology, i.e. the existence of several terrace levels connected by steep slopes, however, suggest that bay-mouth spit development is not only controlled by local factors like wave-climate, nearshore bathymetry and sediment availability, but may reflect regional patterns of relative sea-level changes and climate development.

Sedimentary architecture of Potter Cove gravel-spit system

The Potter Cove spit comprises two terrace levels, located around 3.5 m and 0.8 m amsl, respectively (Figure 9). Both terraces are characterized by a shallow ridge and swale

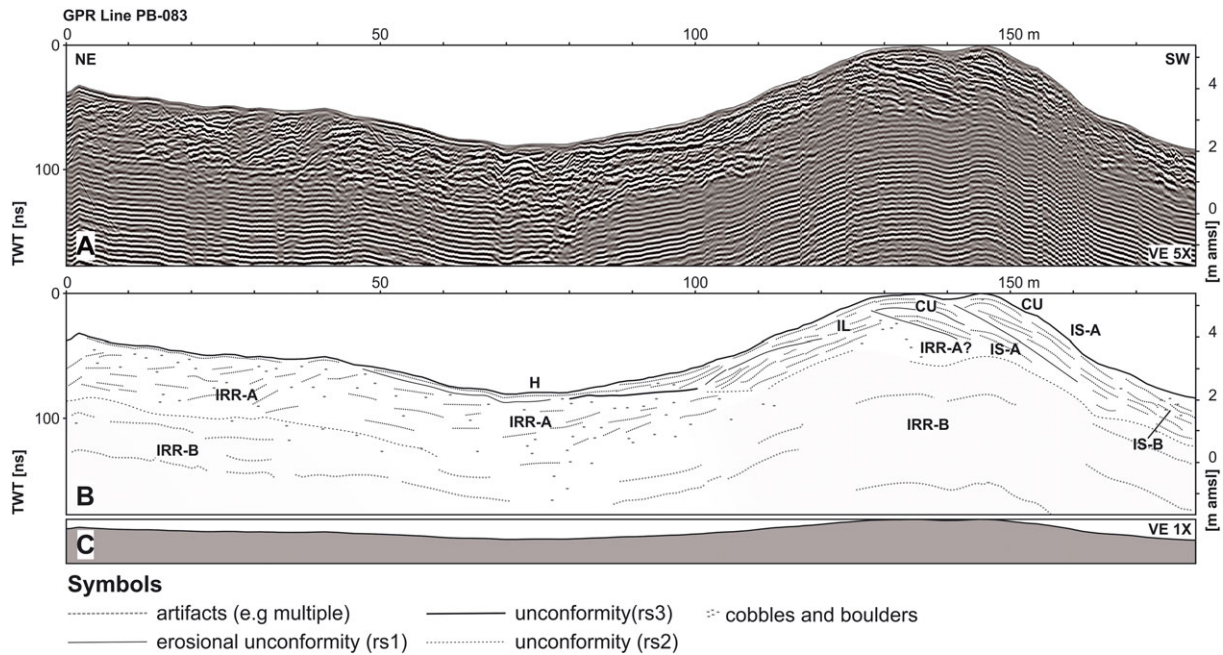


Figure 7. (A) GPR line PB-083. For location see Figure 2. (B) Interpretation of (A). For a detailed discussion of radar facies and sediment geometries see text and Table I. (C) Along-transect topography without vertical exaggeration. [Colour figure can be viewed at wileyonlinelibrary.com]

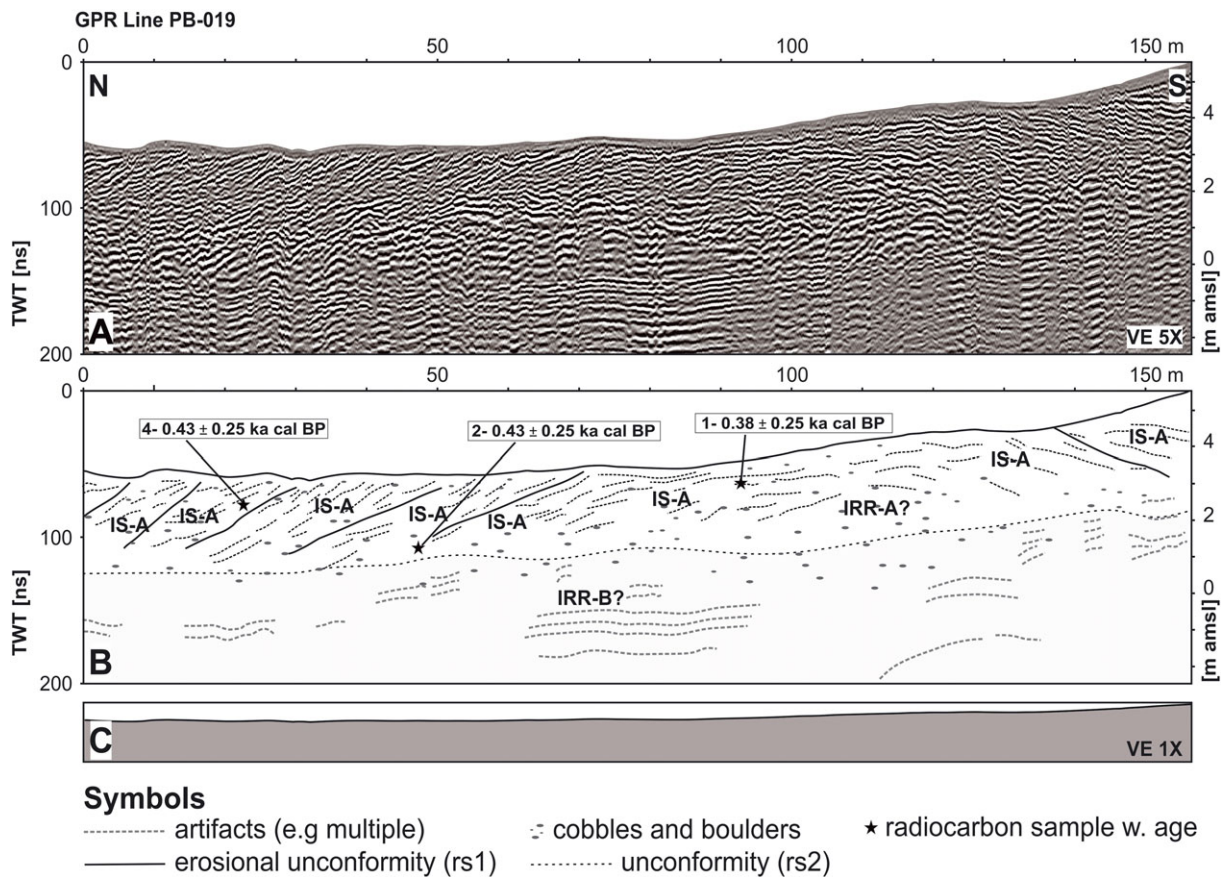


Figure 8. (A) GPR line PB-019 imaging the internal architecture of the upper terrace along the active coastal cliff. For location see Figures 2 and 3. (B) Interpretation of (A). For a detailed discussion of radar facies and sediment geometries see text and Table I. (C) Along-transect topography without vertical exaggeration. [Colour figure can be viewed at wileyonlinelibrary.com]

morphology and are connected by a north-facing slope with superimposed ridges (Figure 2). Morphologically, these terraces form a spit southward-attached to moraines and the volcanic rocks of Potter Peninsula (Figures 1 and 2). In such a coastal configuration, moraines act as both headland anchor and source of sediment which is distributed along the coast by

alongshore currents (Hayes *et al.*, 2010). The western coast of the spit, facing Maxwell Bay, is under erosion and an active coastal cliff developed, documenting ongoing cannibalization and reorganization of the spit system (Figures 2 and 3).

GPR data document that both terrace levels are composed of well-stratified gravel deposits (Figures 3(B), 5 and 8; Table I).

Table I. Radar facies and radar surfaces defined for the interpretation of the GPR data

Radar facies		Characteristics	Interpretation
Inclined			
IS-A		Medium to high amplitude, tabular to slightly convex/concave, moderately continuous. Diffraction hyperbolae. Dip of beds: 2–11°	Planar beds of prograding beach face
IS-B		Medium to high amplitude, discontinuous. Diffraction hyperbolae, partly aligned. Dip of beds: up to 7°	Intertidal gravel sheets
IL		Medium to high amplitude, tabular to slightly convex, moderately continuous. Landward dip: < 12°	Washover beds
Curved			
CU		Low to high amplitude, convex curved, moderately continuous. Landward/seaward dip: < 3.5°	Aggrading storm beds resulting from wave overtopping
Horizontal planar			
H		Low to medium amplitude, planar to slightly concave, moderately to highly continuous.	Backbarrier beds, deposited by meltwater or wind transport
Irregular			
IRR-A		Low to high amplitude, irregular, slightly tabular, numerous diffraction hyperbolae	Poorly sorted glacial till with cobble to boulder size components
IRR-B		Very low amplitude to transparent, irregular, numerous diffraction hyperbolae in uppermost part	Volcanic bedrock. Diffraction hyperbolae are caused by fractures and the sharp, irregular surface of the rock.
Radar surfaces			
rs1		Medium amplitude, moderately continuous, in parts truncation of reflections	Erosional unconformity
rs2		Distinct change of radar facies	Unconformity
rs3		Medium reflection, moderately continuous, numerous diffraction hyperbolae	Contact of beach sediments and substratum (volcanic bedrock or till)

The 1 to 3.5 m thick beach sediments unconformably overlie a basement characterized by irregular GPR reflections and diffraction hyperbolae or appearing transparent in the GPR data (Figures 5 and 6). Whereas transparent parts are interpreted as volcanic bedrock based on outcrop evidence 70 m east to the GPR line PB-009 (Figure 2(B)), diffraction hyperbolae point to the presence of large boulders and cobbles as this is common in the moraines that crop out immediately south of the upper terrace. The contact between spit sediments and underlying moraine deposits remains unclear in the GPR data, most likely due to the similar lithology of both depositional units.

The main sedimentary architectural elements of the upper terrace are packages of divergent seaward-dipping gravelly

beds delimited by erosional unconformities (Figures 5–8). Sedimentary beds dip with up to 11° towards the modern shore and are seen as the result of swash sedimentation at the beach face. Superimposed on the prograding beach sediments of the upper terrace, there are morphological ridges composed of gravel-size sediments (Figures 2(B), 3(C)–(E)). These ridges are interpreted as beach ridges built by waves with run-up heights lower than the ridge crests, according to architectural similarities with gravel beach ridges described from elsewhere in KGI (Lindhorst and Schutter, 2014).

Gravel ridges towards the SW, facing Maxwell Bay, are coarser grained and composed of rounded cobbles (Figure 3(E)). These ridges are amalgamated and superimposed on the SW

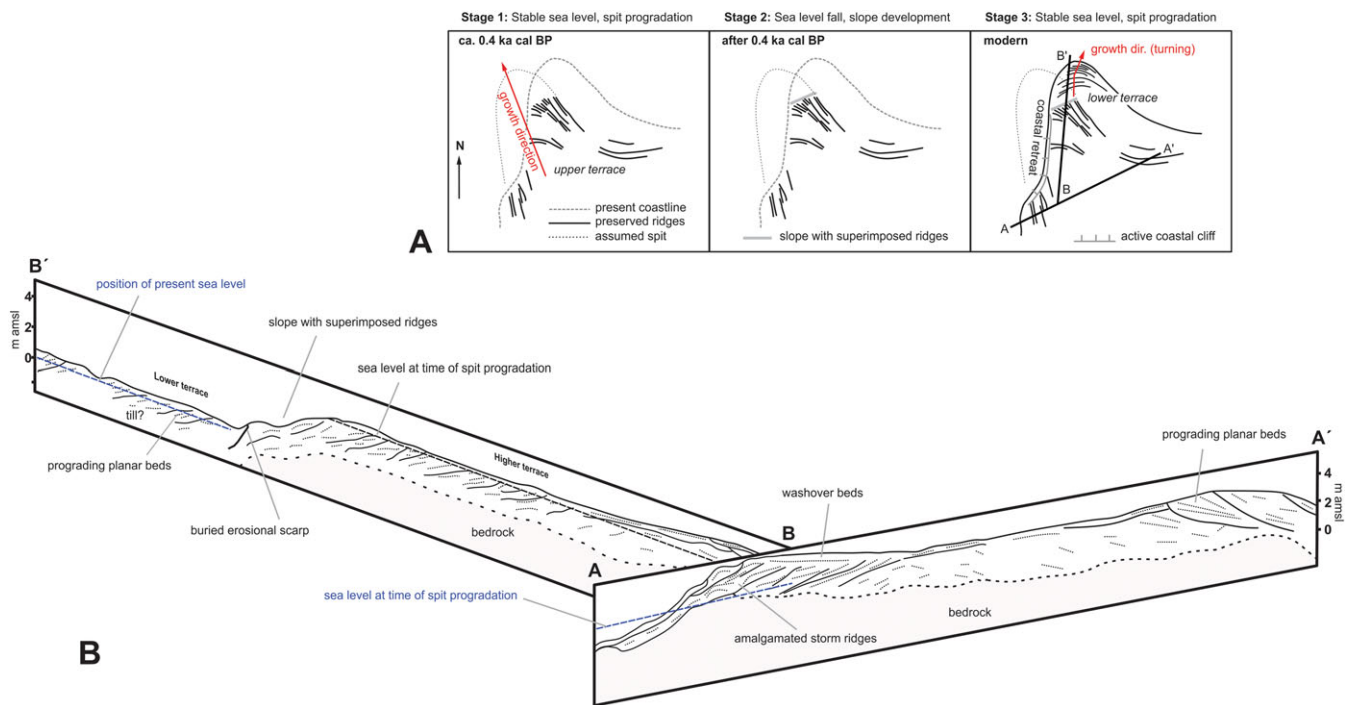


Figure 9. (A) Simplified genetic model for the Potter Cove gravel-spit system through time. Note rotation of the axis of spit progradation from stage 1 to 3. (B) Fence diagram summarizing the main architectural elements of the spit system based on the GPR data. For orientation of cross-sections see (A). [Colour figure can be viewed at wileyonlinelibrary.com]

slope of the upper terrace (Figures 5–7 and Figure 9, stage 1). Ridge internal sediment geometries comprise of convex-aggradational and landward-dipping beds and are interpreted to reflect waves of higher energy that were able to overwash the ridge crests and to transport material to the landward side of the ridge (Lindhorst and Schutter, 2014) (Figure 7). Differences in ridge-internal geometries between the northern and the western slope of the spit are attributed to the higher-energetic wave-climate at the coast facing Maxwell Bay compared with the sheltered coast inside Potter Cove (Figures 1 and 3).

The lower terrace consists of up to 2-m-thick, seaward-dipping gravelly beds, bound into packages by seaward-dipping erosional unconformities. Several arcuate morphological ridges, composed of gravels to cobbles, are superimposed onto the prograding beach deposits of the lower terrace (Figure 2). Seaward-dipping internal beds, as imaged by the GPR, indicate swash deposition with low wave run-up heights even during storms as expected for the comparable sheltered environment inside Potter Cove (Figure 5).

Based on the internal sediment geometries, which predominantly comprise seaward-dipping beds, both terrace levels are interpreted to result from spit progradation (Figure 9). For the upper terrace, striking of beach ridges and internal sediment geometries indicate a NW–SE oriented axis of spit progradation (Figure 9, stage 1). This is slightly different from the lower terrace that started to grow in a northerly direction and subsequently experienced a shift of the direction of progradation towards the NNE over the last decades (Figure 2(C) and Figure 9, stage 3). Even little changes in storm intensity or the predominant angle of wave impact have been shown elsewhere to alter the pattern of spit progradation (Allard *et al.*, 2008; Ashton *et al.*, 2016). Consequently, the still ongoing rotation of the axis of spit progradation is proposed to reflect either a strengthening of westerly storms or the reaction of the system to the observed change of the predominant wind direction during recent decades and a subordinate shift in the direction of (storm-) wave impact onto the coast. Increased storm frequency

or intensity would both result in higher sediment redistribution from the western coast of the spit towards the interior of Potter Cove, due to intensification of the alongshore transport. With the available local meteorological data it remains unclear as to whether the observed shift in the direction of spit progradation is part of a long-term trend or caused by more recent changes in the wind field. On a more regional scale, however, there is evidence that the strength of circumpolar westerly winds increased since the 1970s, especially during the austral summer (van den Broeke, 2000; Turner *et al.*, 2005; Stammerjohn *et al.*, 2008; Montes-Hugo *et al.*, 2009). This is attributed to the poleward movement of the Southern Annular Mode during recent decades, which caused a strengthening of atmospheric low pressure systems around the AP (Marshall *et al.*, 2006). In this context, the observed change in the progradational direction of the spit is likely to reflect larger scale changes in the wind system during the last decades.

Timing of spit evolution

Radiocarbon ages are regarded as similar within the sigma-2 error range (Table II; Figure 2). Seaweed ages from beach sediments, in general, can be regarded as maximum ages, while penguin bones, due to the potential of multiple relocations prior to final burial, represent minimum ages (Watcham *et al.*, 2011). It is therefore assumed that the upper terrace formed not before 0.65 ka cal BP, with a median of the probability distribution around 0.4 ka cal BP (Figure 9, stage 1). Age estimates for the upper terrace fit well with dating results from beach systems at similar elevation in the proximity of the study site (Hall *et al.*, 2010; Simms *et al.*, 2012; Lindhorst and Schutter, 2014). The very recent age of the lower terrace, by contrast, does not allow for absolute age determination using the radiocarbon method. However, given a linearly averaged rate of progradation of 0.44 m yr^{-1} as inferred from historical aerial imagery (Figure 2(C)), the growth of the lower terrace is expected to have started around 1880 CE (0.07 ka BP; Figure 9, stage 3).

Table II. Results of radiocarbon dating

No	Sample ID	Lab ID	Dated material	Coordinates		Altitude	12C/13C ratio [o/oo]	14C age [a BP]	Calibrated age ($\Delta R 791 \pm 121$ a)			
				WGS84 X	UTM 21E Y	m amsl			cal BP (2 σ ranges, 95.4% probability)			Median of prob. [ka]
									Rel. area u. distribution	Range [a]		
1	PB-3000-2	Beta-297365	seaweed	412739	3098106	2.7	-23.8	1540 \pm 30	1.00	110	610	0.38 \pm 0.25
2	PB-3006-1	Beta-304147	seaweed	412742	3098145	1.1	-24.1	1600 \pm 30	0.005	150	160	0.43 \pm 0.25
									0.009	190	220	
									0.98	220	650	
3	PB-PC1.0	Beta-338478	seaweed	412839	3098163	0.6	-21.3	1510 \pm 30	0.001	1	4	0.35 \pm 0.27
									0.99	60	550	
4	Po-23	Beta-431963	penguin bone	412761	3098081	2.3	-22	1600 \pm 30	0.005	150	160	0.43 \pm 0.25
									0.009	190	220	
									0.98	220	650	

Reaction of spit system to accelerated glacier retreat

Based on the direct comparison of radiocarbon ages and dates obtained by means of optical stimulated luminescence, Simms *et al.* (2012) concluded that the formation of beaches now elevated to 7.5–4 m amsl is linked to the last glacial readvance (LGR; 0.45–0.25 ka cal BP; Yoo *et al.*, 2004; Yoo *et al.*, 2009; Simms *et al.*, 2012). These beaches are generally seen as transgressive features, deposited under the circumstances of a relative sea-level rise and increasing storminess during the late stage of the LGR (John and Sugden, 1971; Simms *et al.*, 2012). The internal architecture of the Potter Cove spit system,

however, contradicts this general interpretation and draws a more differentiated picture comprising subsequent phases of coastal progradation interrupted by a rapid fall of relative sea level (Figure 10).

The very gentle seaward slope of the upper terrace (0.6°) is indicative of either rapid spit growth in a very short time period or slow spit growth under a stable relative sea level, i.e. a very low rate of glacio-isostatic adjustment. Due to the large error bars, the radiocarbon ages do not allow for determination of the duration of the older phase of coastal progradation during which the upper terrace formed. However, given that the progradation rate of the lower terrace (0.44 m yr⁻¹) is

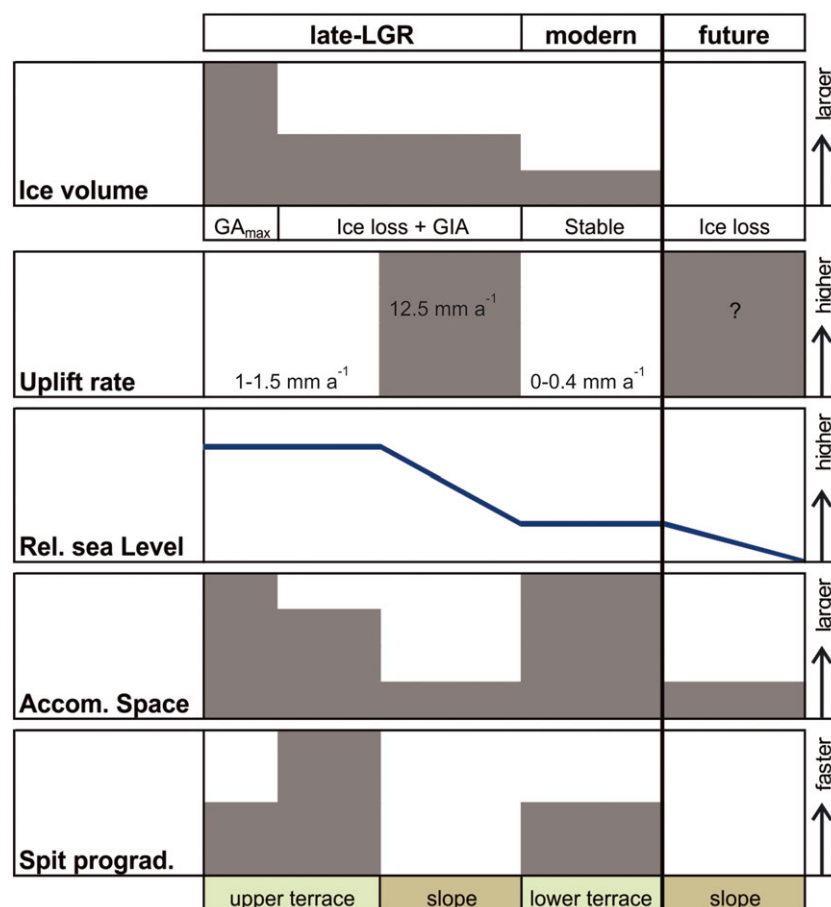


Figure 10. Concept for the interplay of ice volume, glacio-isostatic adjustment (GIA), relative sea-level change, and spit progradation. Note the predicted future development of the system. LGR: last glacial re-advance; GA_{max} : maximum glacier extent during the LGR. [Colour figure can be viewed at wileyonlinelibrary.com]

representative of this setting, sediments of the upper terrace are expected to have been deposited within 200 to 300 years. In combination with the tilt of the upper terrace (c. 0.3 m over a preserved distance of c. 90 m along the former axis of spit progradation) this results in a minimum estimate for the rate of relative sea level fall of 1 to 1.5 mm a⁻¹ during the time of early post-LGR spit progradation. This rate is far below the long-term average uplift of the study area during the entire Holocene, which is estimated at 2.8 to 3 mm a⁻¹ (Bentley *et al.*, 2005; Fretwell *et al.*, 2010). The recent uplift rate, by contrast, is close to zero (Simms *et al.*, 2012; Rülke *et al.*, 2015). This latter is also corroborated by the almost non-existing dip of the lower terrace that indicates no significant uplift since onset of spit progradation, i.e. during the last 100 to 150 years.

The upper terrace is nowadays located at c. 3.5 m amsl, whereas the lower terrace is situated at 0.8 m amsl. Both are connected by a north-facing slope (5° angle) with superimposed beach ridges (Figure 5 and Figure 9, Stage 2). The similarity of internal sediment geometries of the upper and lower terrace indicates comparable elevations with regard to mean sea level during both phases of coastal progradation (Figure 9). The connecting slope is consequently interpreted to have formed during a period of accelerated sea-level fall which amounts to about 2.7 m in total (Figure 9, stage 2). Such a period of accelerated fall of relative sea level is expected to result in a reduction of accommodation space and sediment supply, as indicated by a down-stepping of coastal sediments and the amalgamation of wave-formed ridges on the slope (Figures 5, 9 and 10). Formation of this slope as the result of increased coastal erosion or a longer period of sediment starvation under constant isostatic uplift can be excluded, as amalgamated ridges represent constructive sedimentary features. Comparable morphologies are described from beach-ridge systems of Varanger Peninsula and interpreted as the product of a sudden drop in sea level (Fletcher *et al.*, 1993). Based on modeling results, increased glacio-isostatic uplift in reaction to glacier retreat is assumed for the time following the maximal glacier advance of the LGR, i.e. after around 0.35 ka BP (1600 CE, Simms *et al.*, 2012). The results of these rebound models further show that a reduction of 16 to 22% in ice volume is sufficient to explain about 2.5 m of uplift within 250 years until the mid-19th century.

Summarizing, progradation of polar gravel spits as exemplarily observed in the Potter Cove spit system, is bound to phases of comparable low rates of glacio-isostatic uplift and a resulting stable relative sea level. The morphology of the Potter Cove spit system, with two terrace levels connected by a steep slope with superimposed amalgamated beach ridges, is seen to archive two phases of coastal progradation separated by an abrupt increase in the rate of local glacio-isostatic uplift in reaction to deglaciation after the last glacial re-advance. Based on these findings, a concept for the interplay of ice volume, glacio-isostatic adjustment, relative sea level, and spit progradation is presented (Figure 10). This concept not only explains the morphological and sedimentological characteristics of the Potter Cove system, but also allows predicting future developments of comparable systems elsewhere.

Conclusions

Sedimentary architecture and development of a polar gravel-spit system have been revealed based on ground-penetrating radar data and topographical data, historical aerial imagery and radiocarbon ages. Morphology and internal sediment geometries document changes in the rate of glacio-isostatic uplift between 1 and 1.5 mm and 12.5 mm a⁻¹ on multi-decadal to

centennial time scales. Based on the proposed interplay of fast changes in the rate of crustal relaxation and modes of beach sedimentation, a concept for the interaction of isostatic coastal uplift and spit development has been presented. This concept does not only explain the observed architecture of the spit system but bears implications for the expected future development of similar beach systems in KGI and elsewhere in comparable settings. Accelerated glacier retreat and reduction in ice volume of inland ice shields during recent decades is expected to cause a significant increase in the rate of isostatic uplift and therefore relative sea-level fall during the next decades. The current phase of coastal progradation is expected to terminate in the near future and to be replaced by the development of steep slopes with superimposed amalgamated ridges due to the reduction in accommodation space.

Acknowledgements—We acknowledge funding by the German Research Foundation (DFG project Li2005/1-1 to SL) in the framework of the DFG-priority program 1158 'Antarctic Research with comparative investigations in Arctic ice areas' and support by the Alfred Wegener Institute (AWI), Helmholtz Centre PACES II (Polar Regions and Coasts in the changing Earth System). PHB, UF and GK were funded as well by IMCONet (FP7 IRSES, action no. 319718). SL and IS thank the crews of the Argentine research station 'Carlini' and the adjoined German Dallmann-Labor (AWI) during the 2010 and 2011 field seasons for their cordial hospitality and invaluable logistical support. We also thank KM Stange for his comments, which improved an early version of this manuscript. The manuscript has been significantly improved by the detailed and thorough reviews made by two anonymous reviewers.

Supplementary data

Ground-penetrating radar data obtained in the framework of this study are available from the data depository PANGAEA: (Lindhorst and Schutter, 2013), <https://doi.pangaea.de/10.1594/PANGAEA.825658>

References

- Allard J, Bertin X, Chaumillon E, Pouget F. 2008. Sand spit rhythmic development: a potential record of wave climate variations? Arçay Spit, western coast of France. *Marine Geology* **253**: 107–131. <https://doi.org/10.1016/j.margeo.2008.05.009>.
- Ashton AD, Nienhuis J, Ells K. 2016. On a neck, on a spit: controls on the shape of free spits. *Earth Surface Dynamics* **4**: 193–210. <https://doi.org/10.5194/esurf-4-193-2016>.
- Bañón M, Justel A, Velázquez D, Quesada A. 2013. Regional weather survey on Byers Peninsula, Livingston Island, South Shetland Islands, Antarctica. *Antarctic Science* **25**: 146–156. <https://doi.org/10.1017/S0954102012001046>.
- Baroni C, Orombelli G. 1991. Holocene raised beaches at Terra Nova Bay, Victoria Land, Antarctica. *Quaternary Research* **36**: 157–177. [https://doi.org/10.1016/0033-5894\(91\)90023-X](https://doi.org/10.1016/0033-5894(91)90023-X).
- Bentley MJ, Hodgson DA, Smith JA, Cox NJ. 2005. Relative sea level curves for the South Shetland Islands and Marguerite Bay, Antarctic Peninsula. *Quaternary Science Reviews* **24**: 1203–1216. <https://doi.org/10.1016/j.quascirev.2004.10.004>.
- Berkman PA, Forman SL. 1996. Pre-bomb radiocarbon and the reservoir correction for calcareous marine species in the Southern Ocean. *Geophysical Research Letters* **23**: 363–366.
- Björck S, Hjort C., Ingólfsson, O., Skog, G. 1991. Radiocarbon dates from the Antarctic Peninsula region — problems and potential. In *Radiocarbon dating: recent applications and future potential*, Lowe JJ (ed). Quaternary Proceedings. Quaternary Research Association: Cambridge, UK; 55–65.
- Bluck BJ, Ward JD, Spaggiari R. 2001. Gravel beaches of southern Namibia. In *Ecology and Geomorphology of Coastal Shingle*, Randall RE, Barnes RSK, Neal A, Packham JR (eds). Westbury Academic Scientific Publishing: Westbury, Otley, West Yorks, UK; 56–76.

- Braun M, Saurer H, Gossmann H. 2004. Climate, energy fluxes and ablation rates on the ice cap of King George Island. *Pesquisa Antártica Brasileira* **4**: 87–103.
- Braun M, Saurer H, Vogt S, Simões JC, Goßmann H. 2001. The influence of large-scale atmospheric circulation on the surface energy balance of the King George Island ice cap. *International Journal of Climatology* **21**: 21–36. <https://doi.org/10.1002/joc.563>.
- Bristow C. 1995. Facies analysis in the Lower Greensand using ground-penetrating radar. *Journal of the Geological Society of London* **152**: 591–598. <https://doi.org/10.1144/gsjgs.152.4.0591>.
- Bujalesky GG, Gonzalez Bonorino G. 2015. El Paramo transgressive gravel spit, Tierra del Fuego, Argentina. In *Sand and Gravel Spits*, Randazzo G, Jackson DWT, Cooper JAG (eds). Springer International Publishing: Cham; 37–50.
- Burningham H. 2015. Gravel spit-inlet dynamics: Orford Spit, UK. In *Sand and Gravel Spits*, Randazzo G, Jackson DWT, Cooper JAG (eds). Springer International Publishing: Cham; 51–65.
- Clapperton CM, Sugden DE. 1988. Holocene glacier fluctuations in South America and Antarctica. *Quaternary Science Reviews* **7**: 185–198. [https://doi.org/10.1016/0277-3791\(88\)90005-4](https://doi.org/10.1016/0277-3791(88)90005-4).
- Cook AJ, Fox AJ, Vaughan DG, Ferrigno JG. 2005. Retreating Glacier Fronts on the Antarctic Peninsula over the Past Half-Century. *Science* **308**: 541–544. <https://doi.org/10.1126/science.1104235>.
- Cooper JAG, Jackson DWT, Randazzo G. 2015. Introduction. In *Sand and Gravel Spits*, Randazzo G, Jackson DWT, Cooper JAG (eds). Springer International Publishing: Cham; vii–ix.
- Curl JE. 1980. A glacial history of the South Shetland Islands, Antarctica. In *Institute of Polar Studies Report No. 63*. The Ohio State University: Ohio, USA; 129.
- Deregibus D, Scharf FK, Pasotti F, Ruiz Barlett E, Servetto N, Abele D. 2015. IMCONet Research Areas Map of Potter Cove, King-George Island (l. 25 de Mayo), with links to maps. *PANGAEA*. <https://doi.org/10.1594/PANGAEA.853859>.
- Evans OF. 1942. The origin of spits, bars, and related structures. *The Journal of Geology* **50**: 846–865. <https://doi.org/10.1086/625087>.
- Falk U, Sala H. 2015. Winter melt conditions of the inland ice cap on King George Island, Antarctic Peninsula. *Erdkunde* **69**: 341–363. <https://doi.org/10.3112/erdkunde.2015.04.04>.
- Fletcher CH, III, Fairbridge RW, Møller JJ, Long AJ. 1993. Emergence of the Varanger Peninsula, Arctic Norway, and climate changes since deglaciation. *The Holocene* **3**: 116–127. <https://doi.org/10.1177/095968369300300203>.
- Forbes D, Taylor R. 1987. Coarse-grained beach sedimentation under paraglacial conditions, Canadian Atlantic coast. In *Glaciated Coasts*, FitzGerald DM, Rosen PS (eds). Academic Press: San Diego; 51–86.
- Forbes DL, Orford JD, Carter RWG, Shaw J, Jennings SC. 1995. Morphodynamic evolution, self-organisation, and instability of coarse-clastic barriers on paraglacial coasts. *Marine Geology* **126**: 63–85. [https://doi.org/10.1016/0025-3227\(95\)00066-8](https://doi.org/10.1016/0025-3227(95)00066-8).
- Fretwell PT, Hodgson DA, Watcham EP, Bentley MJ, Roberts SJ. 2010. Holocene isostatic uplift of the South Shetland Islands, Antarctic Peninsula, modelled from raised beaches. *Quaternary Science Reviews* **29**: 1880–1893. <https://doi.org/10.1016/j.quascirev.2010.04.006>.
- Gawthorpe RL, Collier REL, Alexander J, Bridge JS, Leeder MR. 1993. Groundpenetrating radar: application to sandbody geometry and heterogeneity studies. In *Characterization of Fluvial and Aeolian Reservoirs*, North CP, Prosser DJ (eds). Geological Society of London Special Publications: London; 421–432.
- Griffith TW, Anderson JB. 1989. Climatic control of sedimentation in bays and fjords of the northern Antarctic Peninsula. *Marine Geology* **85**: 181–204. [https://doi.org/10.1016/0025-3227\(89\)90153-9](https://doi.org/10.1016/0025-3227(89)90153-9).
- Hall BL. 2010. Holocene relative sea-level changes and ice fluctuations in the South Shetland Islands. *Global and Planetary Change* **74**: 15–26. <https://doi.org/10.1016/j.gloplacha.2010.07.007>.
- Hall BL, Henderson GM, Baroni C, Kellogg TB. 2010. Constant Holocene Southern-Ocean 14C reservoir ages and ice-shelf flow rates. *Earth and Planetary Science Letters* **296**: 115–123. <https://doi.org/10.1016/j.epsl.2010.04.054>.
- Hall BL, Perry ER. 2004. Variations in ice rafted detritus on beaches in the South Shetland Islands: a possible climate proxy. *Antarctic Science* **16**: 339–344. <https://doi.org/10.1017/S0954102004002147>.
- Hass HC, Kuhn G, Monien P, Brumsack H-J, Forwick M. 2010. Climate fluctuations during the past two millennia as recorded in sediments from Maxwell Bay, South Shetland Islands, West Antarctica. *Geological Society, London, Special Publications* **344**: 243–260. <https://doi.org/10.1144/sp344.17>.
- Hayes MO, Michel J, Betenbaugh DV. 2010. The intermittently exposed, coarse-grained gravel beaches of Prince William Sound, Alaska: comparison with open-ocean gravel beaches. *Journal of Coastal Research* **26**: 4–30. <https://doi.org/10.2112/08-1071.1>.
- Jerosch K, Pehlke H, Monien P, Scharf F, Weber L, Kuhn G, Braun MH, Abele D. 2018. Benthic meltwater fjord habitats formed by rapid glacier recession on King George Island, Antarctica. *Philosophical Transactions of the Royal Society A* **376**. <https://doi.org/10.1098/rsta.2017.0178>.
- John BS, Sugden DE. 1971. Raised marine features and phases of glaciation in the South Shetland Islands. *British Antarctic Survey Bulletin* **24**: 45–111.
- Kejna M, Arażny A, Sobota I. 2013. Climatic change on King George Island in the years 1948–2011. *Polish Polar Research* **34**: 213–235. <https://doi.org/10.2478/popore-2013-0004>.
- Lemoine FG, Kenyon SC, Factor JK, Trimmer RG, Pavlis NK, Chinn DS, Cox CM, Klosko SM, Luthcke SB, Torrence MH, Wang YM, Williamson RG, Pavlis EC, Rapp RH, Olson TR. 1998. The Development of the Joint NASA GSFC and NIMA Geopotential Model EGM96. In *NASA Technical Paper TP-1998-206861*. NASA Goddard Space Flight Center Greenbelt: USA; 584.
- Lim CH, Lettmann K, Wolff J-O. 2013. Numerical study on wave dynamics and wave-induced bed erosion characteristics in Potter Cove, Antarctica. *Ocean Dynamics* **63**: 1151–1174. <https://doi.org/10.1007/s10236-013-0651-z>.
- Lindhorst S, Betzler C, Hass HC. 2008. The sedimentary architecture of a Holocene barrier spit (Sylt, German Bight): swash-bar accretion and storm erosion. *Sedimentary Geology* **206**: 1–16. <https://doi.org/10.1016/j.sedgeo.2008.02.008>.
- Lindhorst S, Schutter I. 2013. 47 ground-penetrating radar lines of Area 4 – gravel- spit system from Potter Cove, King George Island, Antarctic Peninsula. *PANGAEA*. <https://doi.org/10.1594/PANGAEA.825658>.
- Lindhorst S, Schutter I. 2014. Polar gravel beach-ridge systems: sedimentary architecture, genesis, and implications for climate reconstructions (South Shetland Islands/Western Antarctic Peninsula). *Geomorphology* **221**: 187–203. <https://doi.org/10.1016/j.geomorph.2014.06.013>.
- Marshall GJ, Orr A, Lipzig NPMv, King JC. 2006. The impact of a changing Southern Hemisphere Annular Mode on Antarctic Peninsula summer temperatures. *Journal of Climate* **19**: 5388–5404. <https://doi.org/10.1175/jcli3844.1>.
- Mason OK. 2010. Beach Ridge Geomorphology at Cape Grinnell, northern Greenland: a less icy Arctic in the Mid-Holocene. *Geografisk Tidsskrift-Danish Journal of Geography* **110**: 337–355. <https://doi.org/10.1080/00167223.2010.10669515>.
- Meredith MP, King JC. 2005. Rapid climate change in the ocean west of the Antarctic Peninsula during the second half of the 20th century. *Geophysical Research Letters* **32**: 1–5. <https://doi.org/10.1029/2005GL024042>.
- Milliken KT, Anderson JB, Wellner JS, Bohaty SM, Manley PL. 2009. High-resolution Holocene climate record from Maxwell Bay, South Shetland Islands, Antarctica. *Geological Society of America Bulletin* **121**: 1711–1725. <https://doi.org/10.1130/b26478.1>.
- Mitchum RM, Vail PR, Sangree JB. 1977. Stratigraphic interpretation of seismic reflection patterns in depositional sequences. In *Seismic Stratigraphy—Applications to Hydrocarbon Exploration*, Payton CE (ed). American Association of Petroleum Geologists Memoir: Tulsa, USA; **16**: 117–133.
- Møller JJ, Yevzerov VY, Kolka VV, Corner GD. 2002. Holocene raised-beach ridges and sea-ice-pushed boulders on the Kola Peninsula, northwest Russia: indicators of climatic change. *The Holocene* **12**: 169–176. <https://doi.org/10.1191/0959683602hl532rp>.
- Montes-Hugo M, Doney SC, Ducklow HW, Fraser W, Martinson D, Stammerjohn SE, Schofield O. 2009. Recent changes in phytoplankton communities associated with rapid regional climate change along the western Antarctic Peninsula. *Science* **323**: 1470–1473. <https://doi.org/10.1126/science.1164533>.
- Navarro FJ, Jonsell UY, Corcuera MI, Martín-Español A. 2013. Decelerated mass loss of Hurd and Johnsons Glaciers, Livingston Island,

- Antarctic Peninsula. *Journal of Glaciology* **59**: 115–128. <https://doi.org/10.3189/2013jog12j144>.
- Nielsen L, Bendixen M, Kroon A, Hede MU, Clemmensen LB, Weßling R, Elberling B. 2017. Sea-level proxies in Holocene raised beach ridge deposits (Greenland) revealed by ground-penetrating radar. *Scientific Reports* **7**: 1–8. <https://doi.org/10.1038/srep46460>.
- Nielsen LH, Johannessen PN. 2009. Facies architecture and depositional processes of the Holocene – recent accretionary forced regressive Skagen spit system, Denmark. *Sedimentology* **56**: 935–968. <https://doi.org/10.1111/j.1365-3091.2008.01007.x>.
- Ó Cofaigh C, Davies BJ, Livingstone SJ, Smith JA, Johnson JS, Hocking EP, Hodgson DA, Anderson JB, Bentley MJ, Canals M, Domack E, Dowdeswell JA, Evans J, Glasser NF, Hillenbrand C-D, Larter RD, Roberts SJ, Simms AR. 2014. Reconstruction of ice-sheet changes in the Antarctic Peninsula since the Last Glacial Maximum. *Quaternary Science Reviews* **100**: 87–110. <https://doi.org/10.1016/j.quascirev.2014.06.023>.
- Orford JD, Forbes DL, Jennings SC. 2002. Organisational controls, typologies and time scales of paraglacial gravel-dominated coastal systems. *Geomorphology* **48**: 51–85. [https://doi.org/10.1016/S0169-555X\(02\)00175-7](https://doi.org/10.1016/S0169-555X(02)00175-7).
- Osmanoğlu B, Braun M, Hock R, Navarro FJ. 2013. Surface velocity and ice discharge of the ice cap on King George Island, Antarctica. *Annals of Glaciology* **54**: 111–119. <https://doi.org/10.3189/2013AoG63A517>.
- Otvos EG. 2012. Coastal barriers — nomenclature, processes, and classification issues. *Geomorphology* **139**: 39–52. <https://doi.org/10.1016/j.geomorph.2011.10.037>.
- Pallàs R, James T, Sàbat F, Vilaplana J, Grant D, Ricci C. 1997. Holocene uplift in the South Shetland Islands: evaluation of tectonics and glacio-isostasy. In *The Antarctic Region: Geological Evolution and Processes*, Ricci C (ed). Terra Antarctica Publication: Siena, Italy; 861–868.
- Reimer PJ, Bard E, Bayliss A, Beck JW, Blackwell PG, Ramsey CB, Buck CE, Cheng H, Edwards RL, Friedrich M, Grootes PM, Guilderson TP, Hafildason H, Hajdas I, Hatté C, Heaton TJ, Hoffmann DL, Hogg AG, Hughen KA, Kaiser KF, Kromer B, Manning SW, Niu M, Reimer RW, Richards DA, Scott EM, Southon JR, Staff RA, Turney CSM, van der Plicht J. 2013. IntCal13 and Marine13 radiocarbon age calibration curves 0–50,000 Years cal BP. *Radiocarbon* **55**: 1869–1887. https://doi.org/10.2458/azu_js_rc.55.16947.
- Rückamp M, Braun M, Suckro S, Blindow N. 2011. Observed glacial changes on the King George Island ice cap, Antarctica, in the last decade. *Global and Planetary Change* **79**: 99–109. <https://doi.org/10.1016/j.gloplacha.2011.06.009>.
- Rülke A, Dietrich R, Capra A, Cisak J, Dongchen E, Eiken T, Fox A, Hothem LD, Johnston G, Malaimani EC, Matveev AJ, Milinevsky G, Schenke H-W, Shibuya K, Sjöberg LE, Zakrajsek A, Fritsche M, Groh A, Knöfel C, Scheinert M. 2015. The Antarctic Regional GPS Network Densification: Status and Results. In *IAG 150 Years: Proceedings of the IAG Scientific Assembly in Postdam, Germany, 2013*, Rizos C, Willis P (eds). Springer International Publishing: Cham; 133–139.
- Santana E, Dumont JF. 2007. Granulometry of pebble beach ridges in Fort William Point, Greenland Island, Antarctic Peninsula; a possible result from Holocene climate fluctuations. Antarctica: A keystone in changing world—Online proceeding of the 10th ISAES. *USGS Open File Report. Short Research Paper 027* **1047**: 1–4.
- Schloss IR, Abele D, Moreau S, Demers S, Bers AV, González O, Ferreyra GA. 2012. Response of phytoplankton dynamics to 19-year (1991–2009) climate trends in Potter Cove (Antarctica). *Journal of Marine Systems* **92**: 53–66. <https://doi.org/10.1016/j.jmarsys.2011.10.006>.
- Schloss IR, Wasilowska A, Dumont D, Almandoz GO, Hernando MP, Michaud-Tremblay CA, Saravia L, Rzepecki M, Monien P, Monien D, Kopczyńska EE, Bers AV, Ferreyra GA. 2014. On the phytoplankton bloom in coastal waters of southern King George Island (Antarctica) in January 2010: an exceptional feature? *Limnology and Oceanography* **59**: 195–210. <https://doi.org/10.4319/lo.2014.59.1.0195>.
- Schoene T, Pohl M, Zakrajsek AF, Schenke H-W. 1998. Tide gauge measurements - a contribution for the long term monitoring of the sea level. In *The Potter Cove Coastal Ecosystem, Antarctica, Berichte zur Polarforschung*, Wiencke C, Ferreyra G, Arntz W, Rinaldi C (eds). Alfred Wegener Institute for Polar and Marine Research: Bremerhaven, Germany; 12–14.
- Simkins LM, Simms AR, Dewitt R. 2015. Assessing the link between coastal morphology, wave energy and sea ice throughout the Holocene from Antarctic raised beaches. *Journal of Quaternary Science* **30**: 335–348. <https://doi.org/10.1002/jqs.2782>.
- Simms AR, Ivins ER, DeWitt R, Kouremenos P, Simkins LM. 2012. Timing of the most recent Neoglacial advance and retreat in the South Shetland Islands, Antarctic Peninsula: insights from raised beaches and Holocene uplift rates. *Quaternary Science Reviews* **47**: 41–55. <https://doi.org/10.1016/j.quascirev.2012.05.013>.
- Simms AR, Milliken KT, Anderson JB, Wellner JS. 2011. The marine record of deglaciation of the South Shetland Islands, Antarctica since the Last Glacial Maximum. *Quaternary Science Reviews* **30**: 1583–1601. <https://doi.org/10.1016/j.quascirev.2011.03.018>.
- SMN. 2016. *SMN: Meteorological observations at Carlini base*. AMS: Argentina, Buenos Aires <http://www.smn.gov.ar>, date: 01.01.2016.
- Stammerjohn SE, Martinson DG, Smith RC, Yuan X, Rind D. 2008. Trends in Antarctic annual sea ice retreat and advance and their relation to El Niño–Southern Oscillation and Southern Annular Mode variability. *Journal of Geophysical Research, Oceans* **113**: 1–20. <https://doi.org/10.1029/2007JC004269>.
- St-Hilaire-Gravel D, Bell TJ, Forbes DL. 2010. Raised gravel beaches as proxy indicators of past sea-ice and wave conditions, Lowther Island, Canadian Arctic Archipelago. *Arctic* **63**: 213–226.
- St-Hilaire-Gravel D, Forbes DL, Bell T. 2012. Multitemporal analysis of a gravel-dominated coastline in the Central Canadian Arctic Archipelago. *Journal of Coastal Research* **28**(2): 421–441. <https://doi.org/10.2112/jcoastres-d-11-00020.1>.
- St-Hilaire-Gravel D, Forbes DL, Bell T. 2015. Evolution and morphodynamics of a prograded beach-ridge foreland, northern bafin island, canadian arctic archipelago. *Geografiska Annaler. Series A, Physical Geography* **97**: 615–631.
- Strzelecki MC, Long AJ, Lloyd JM. 2015. Post-Little Ice Age development of a high arctic paraglacial beach complex. *Permafrost and Periglacial Processes* **28**: 4–17. <https://doi.org/10.1002/ppp.1879>.
- Strzelecki MC, Long AJ, Lloyd JM, Matecki J, Zagórski P, Pawłowski Ł, Jaskólski MW. 2018. The role of rapid glacier retreat and landscape transformation in controlling the post-Little Ice Age evolution of paraglacial coasts in central Spitsbergen (Billefjorden, Svalbard). *Land Degradation and Development* **29**: 1962–1978. <https://doi.org/10.1002/ldr.2923>.
- Stuiver M, Reimer PJ. 1993. Extended 14C Data base and revised CALIB 3.0 14C age calibration program. *Radiocarbon* **35**: 215–230. <https://doi.org/10.1017/S0033822200013904>.
- Sugden DE, John BS. 1973. The ages of glacier fluctuations in the South Shetland Islands, Antarctica. In *Palaeoecology of Africa, the Surrounding Islands and Antarctica*, van Zinderen Bakker EM (ed). Balkema: Cape Town; 141–159.
- Tamura T. 2012. Beach ridges and prograded beach deposits as palaeoenvironment records. *Earth-Science Reviews* **114**: 279–297. <https://doi.org/10.1016/j.earscirev.2012.06.004>.
- Tucker ME. 1996. *Sedimentary Rocks in the Field*. John Wiley & Sons: Chichester.
- Turner J, Colwell SR, Marshall GJ, Lachlan-Cope TA, Carleton AM, Jones PD, Lagun V, Reid PA, Iagovkina S. 2004. The SCAR READER Project: toward a high-quality database of mean antarctic meteorological observations. *Journal of Climate* **17**: 2890–2898. [https://doi.org/10.1175/1520-0442\(2004\)017<2890:tsrpta>2.0.co;2](https://doi.org/10.1175/1520-0442(2004)017<2890:tsrpta>2.0.co;2).
- Turner J, Lachlan-Cope T, Colwell S, Marshall GJ. 2005. A positive trend in western Antarctic Peninsula precipitation over the last 50 years reflecting regional and Antarctic-wide atmospheric circulation changes. *Annals of Glaciology* **41**: 85–91.
- van den Broeke MR. 2000. The semi-annual oscillation and Antarctic climate. Part 4: A note on sea ice cover in the Amundsen and Bellingshausen Seas. *International Journal of Climatology* **20**: 455–462.
- Vaughan DG. 2006. Recent trends in melting conditions on the Antarctic Peninsula and their implications for ice-sheet mass balance and sea level. *Arctic, Antarctic, and Alpine Research* **38**: 147–152. [https://doi.org/10.1657/1523-0430\(2006\)038\[0147:RTIMCO\]2.0.CO;2](https://doi.org/10.1657/1523-0430(2006)038[0147:RTIMCO]2.0.CO;2).

- Watcham EP, Bentley MJ, Hodgson DA, Roberts SJ, Fretwell PT, Lloyd JM, Larter RD, Whitehouse PL, Leng MJ, Monien P, Moreton SG. 2011. A new Holocene relative sea level curve for the South Shetland Islands, Antarctica. *Quaternary Science Reviews* **30**: 3152–3170. <https://doi.org/10.1016/j.quascirev.2011.07.021>.
- Wöfl A-C, Wittenberg N, Feldens P, Hass HC, Betzler C, Kuhn G. 2016. Submarine landforms related to glacier retreat in a shallow Antarctic fjord. *Antarctic Science* **28**: 475–486. <https://doi.org/10.1017/S0954102016000262>.
- Yoo K-C, Yoon HI, Kim J-K, Khim B-K. 2009. Sedimentological, geochemical and palaeontological evidence for a neoglacial cold event during the late Holocene in the continental shelf of the northern South Shetland Islands, West Antarctica. *Polar Research* **28**: 177–192. <https://doi.org/10.1111/j.1751-8369.2009.00109.x>.
- Yoon HI, Woo Han M, Park B-K, Oh J-K, Soon-Keun C. 1997. Glaciomarine sedimentation and palaeo-glacial setting of Maxwell Bay and its tributary embayment, Marian Cove, South Shetland Islands, West Antarctica. *Marine Geology* **140**: 265–282. [https://doi.org/10.1016/S0025-3227\(97\)00028-5](https://doi.org/10.1016/S0025-3227(97)00028-5).
- Yoon HI, Yoo K-C, Park B-K, Kim Y, Khim B-K, Kang C-Y. 2004. The origin of massive diamicton in Marian and Potter coves, King George Island, West Antarctica. *Geosciences Journal* **8**: 1–10. <https://doi.org/10.1007/bf02910274>.